

# ELECTRON DENSITY DISTRIBUTION IMAGING IN COMPTON SCATTERING TOMOGRAPHY

O. O. Adejumo<sup>1\*</sup>G.G.O Egbedokun<sup>2</sup> and F. A Balogun<sup>3</sup>

<sup>1</sup>Department of Physics and Solar Energy, Bowen University, Iwo, Nigeria.

<sup>2</sup>Department of Computer Studies, The Polytechnic, Ibadan, Nigeria

<sup>3</sup>Centre for Energy Research and Development, Obafemi Awolowo University, Ile-Ife, Nigeria

Email: \*oladipoadejumo@yahoo.com

## Abstract

Interest in this work was prompted by the potential advantages of the use of Compton scattering tomography, CST method over X-ray computed tomography, CT. The CST method can image directly the electron density of materials using transmitted scattered photons rather than attenuation coefficients as in the case of CT, also the detector does not have to be on opposite sides of the source and object as is required in CT technique. This flexibility is very useful when images of objects buried under the ground are desired. Imaging of the electron density distribution of materials by recording the number of scattered photons as a function of energy and detector position was carried out. From the image reconstruction formula, a computer program written in C++ language was developed to generate the electron density function of the point scatterer. From this generated data, phantom images were obtained by plotting the electron density function at varying scattering circles radii versus the scattering angle  $\phi$  using Microsoft Excel. Observation of these images reveals that at scattering circle radii of about 10cm, better image details emerged. The implication of this should lead to the realization of the optimal positioning of the CST system for real-time scan situations. This preliminary step towards the real-time development of the CST system as reported in this work should open the gate for new and better possibilities in tomographic methods.

**Keywords:** Compton Scattering Tomography, CST; Image Reconstruction; Electron Density; Attenuation; Line Integrals.

## 1. Introduction

In the  $\gamma$ -ray energy regime from about 0.1 to 1.0 MeV, and for materials with low to intermediate atomic numbers, the dominant interaction mechanism in matter is Compton scattering. Early pioneers of the use of Compton scattering in imaging applications include Lale (1959), Clarke et al. (1976), and in 1971, Farmer and Collins made use of the energy spectrum of scattered gamma radiation measured by a germanium detector. Wang et al.,(1999), presented an improved form of the detector response function and validated the transform method proposed by Norton for the Compton scattering image reconstruction. Cebeiro et al., (2017) showed that the standard CST can be 'improved' in some particular sense by 'doubling' the scanning mechanism. Adejumo et al., (2011) opined that CST techniques can be applied in soil studies. The attraction of Compton Scattering Imaging, CSI lies in its ability to image directly the electron density distribution of materials rather than

the attenuation coefficients of transmitted photons as is the case with computed tomography, CT; as well as the flexibility it offers in the positioning of its detector, which does not have to be on opposite sides of the source as is required in transmission imaging. These give the CSI method potential advantages over X-ray transmission CT, especially when images of objects buried under the ground are concerned. In general, CT is the task of reconstructing an unknown function from measurements of its line integrals, and in X-ray transmission CT, this unknown function is the distribution of the linear attenuation coefficient. Compton Scattering Tomography, CST, is a form of tomography in which the unknown function is the local Compton Scattering cross-section. This quantity which is spatially varying (depending on the material's mass density and composition) is related to the local electron density of the material. Unlike the case of X-ray transmission CT, where the tomographic problem is characterized by line integrals defined along a set of overlapping straight lines joining multiple source and detector points, the CST problem of a system under consideration is characterized by line integrals measured over circular paths. Norton, in 1994 showed that neglecting photoelectric absorption, for a  $\gamma$ -ray of known energy, emitted unto an object from a source point S, Compton scattered once, and detected at a point D outside the object, to a very good approximation, the energy loss suffered by the photon upon scattering is a function only of the scattering angle  $\theta$  subtended by the points S and D. When scattering is confined to a plane, the locus of scattering points having the same emitting point S, detecting point D and scattering angle  $\theta$ , or, equivalently, recorded energy,  $E_\theta$  and can be shown to be a circle whose centre and radius is uniquely determined by the three parameters S, D and  $\theta$  (or energy  $E_\theta$ ) (Norton, 1994). When point S is an omnidirectional source of  $\gamma$ -rays, the number of Compton scattered photons recorded at D with particular energy  $E_\theta$  is a (weighted) line integral of the electron density over this circular path. Norton, further showed that in the CST method, a complete set of path integral measurements, generated by recording the scattered photons as a function of energy and detector position, is sufficient to recover the unknown electron density. In the ideal case, where (i) perfect energy and spatial resolution of the detector is assumed; (ii) noise and multiple scattering is neglected; and (iii) insignificant attenuation along the path between the source and scattering point and from that point to the site of the detector is also assumed, the problem is analytically tractable and has an exact solution (Norton, 1994). In the CST problem, departures from the ideal case occur as a result of (i) imposition of limits by the finite energy and spatial resolution of a real detector; (ii) incidence of multiple scattering, which may be arbitrarily reduced by collimating source and detector to one plane; reducing out-of-plane scatter. This is attainable at the expense of a reduction in counting statistics, which increases data acquisition time, and results in an increase in radiation exposure of the sample. This is undesirable, as it is not in line with the ALARA (As Low As Reasonably Achievable) principle of radiation protection in industrial applications. A more significant departure from the ideal is the assumption of negligible attenuation due to Compton scattering along the source-scatterer-detector paths. Hence, in a real situation, the detected scattered signal is modulated by the attenuation factors of pre- and post-scattered radiation. Arendtsz and Hussein, in 1995 opined that these factors are a function of the unknown density of the object, which one is trying to obtain by imaging.

## 2. Methodology

### *Mathematical Formulation*

The CST problem is characterized by the measurements of line integrals over circular paths whose origin can be traced to the locus of points in the X-Y plane from which the source S

and detector D subtend the same scattering angle  $\theta$ . This locus of points is a circle passing through the source and detector (Norton, 1994). Norton in this work in 1994, derived the equation of the scattering circle (after rigorous mathematical manipulations) as:

$$I(R, \phi) = \int_0^\pi d\theta_p \int_0^\infty f(r, \theta_p) \omega(r, \theta_p; R, \phi) dr \delta[r - 2R \cos(\theta_p - \phi)] \quad (1)$$

where  $\delta(\bullet)$  is the 1-D Dirac delta function

R is the radius of the scattering circle

$$\phi = \pi/2 - \theta$$

$f(r, \theta_p)$  is electron density denoted in polar coordinates

$\omega(r, \theta_p; R, \phi)$  is the weighting factor for an ideal situation (when attenuation is ignored)

Kouris et al., in 1982 had shown that in  $\gamma$ -ray emission tomography, the problem of attenuation is more complicated because the integral of the linear attenuation coefficient depends on the distance between the point of emission along the line and the detector.

Norton began the approximate treatment of attenuation by considering the general case in which the weighting function,  $\omega$  is not factorable, i.e., when

$$\omega(r, \theta_p; R, \phi) \neq \omega_1(r, \theta_p) \omega_2(R, \phi)$$

and after incorporating the question of attenuation into the weighting function and much rigorous mathematical manipulations finally obtained the equation for the image of a point scatterer at  $(r_0, \theta_{p0})$  embedded in a uniformly attenuating medium with constant attenuation coefficient,  $\mu$  as

$$f_a(r, \theta_p) = \frac{1}{(2\pi)^2} \int_0^{2\pi} d\phi \int_0^{R_{\max}} R dR \exp\left[\frac{-\mu r_0 (\sin \theta_{p0} - \sin \theta_p)}{\cos(\theta_{p0} - \phi)}\right] h\left[r - r_0 \frac{\cos(\theta_p - \phi)}{\cos(\theta_{p0} - \phi)}\right] \frac{C(\phi; r_0, \theta_{p0})}{\cos^2(\theta_{p0} - \phi)} \quad (2)$$

where  $C(\phi; r_0, \theta_{p0}) \equiv \begin{cases} 1 & \text{when } |\cos(\theta_{p0} - \phi)| > r_0 / 2R_{\max} \\ 0 & \text{otherwise} \end{cases}$

$f_a(r, \theta_p)$  is the object function (point scatterer to be imaged).

Equation 2 above gives the image of the point scatterer at  $(r_0, \theta_{p0})$  embedded in a uniformly attenuating medium with constant attenuation coefficient,  $\mu$

$1/\mu$  is the meanfree path length of a  $\gamma$ -ray in the attenuating medium.

### Compton Scattering Image Reconstruction Algorithm

The equation of the image of a point scatterer, (Eqn 2 above) was first numerically integrated at different values of  $\mu$ . Values of  $\mu = 2/r_0$  and  $\mu = 4/r_0$  were used in developing the image reconstruction algorithm.

#### Image Reconstruction Algorithm

Step

1. Start
2. Set pi  $\rightarrow$  1
3. Set i  $\rightarrow$  0
4. theta  $\rightarrow$  pi \* i
5. phi(i)  $\rightarrow$  90 - theta
6. increment i by 10

7. if  $i \leq 180$  goto step 4
8. Set  $j \rightarrow$
9. Set  $y \rightarrow$
10.  $R \rightarrow 10$
11.  $r0(j) \rightarrow 2 * R * \cos(\text{theta} - \text{phi}(y))$
12.  $\mu(j) \rightarrow 2 / r0(j)$
13.  $a(j) \rightarrow (-\mu(j) * r0(j) * (\sin(80) - \sin(10)) / \cos(80 - \text{phi}(y)))$
14.  $\text{expa}(j) \rightarrow \exp(a(j))$
15.  $\text{Rexpa}(j) \rightarrow R * \text{expa}(j)$
16.  $h(j) \rightarrow \exp(\sin(12.5 / r0(j)) * 12.5 / r0(j))$
17. Increase  $y$  by 1
18. If  $y \leq 150$  then goto step 10
19. Set  $k = 2$
20.  $x \rightarrow k - 1$
21. Set  $\text{thetap} = 0$
22.  $d(x) \rightarrow r0(1) * (\cos(\text{thetap} - \text{phil}(x)) / \cos(80 - \text{phi}(x)))$
23. Increase  $\text{thetap}$  by 10
24. If  $\text{thetap} \leq 180$  then goto step 22
25.  $b(x) \rightarrow (r0(k) - d(x)) * (1 / \text{pow}(\cos(10 - \text{phil}(x)), 2)) * h(k)$
26. Increase  $k$  by 1
27. If  $k \leq 20$  goto step 20
28.  $R \rightarrow 1$
29.  $j \rightarrow 1$
30. Display heading
31. Set  $f(j) = R * \text{Rexpa}(j) * b(j)$
32. Display  $f(j)$  and  $\text{phi}(j)$
33. Increase  $j$  by 1
34. If  $j \leq 20$  goto step 31
35. Increase  $R$  by 1
36. If  $R \leq 15$  goto step 29
37. Stop

### 3. Results

The images of a phantom at scattering circle radii of between 10 and 20cm are shown in Figures 1 to 6 below.

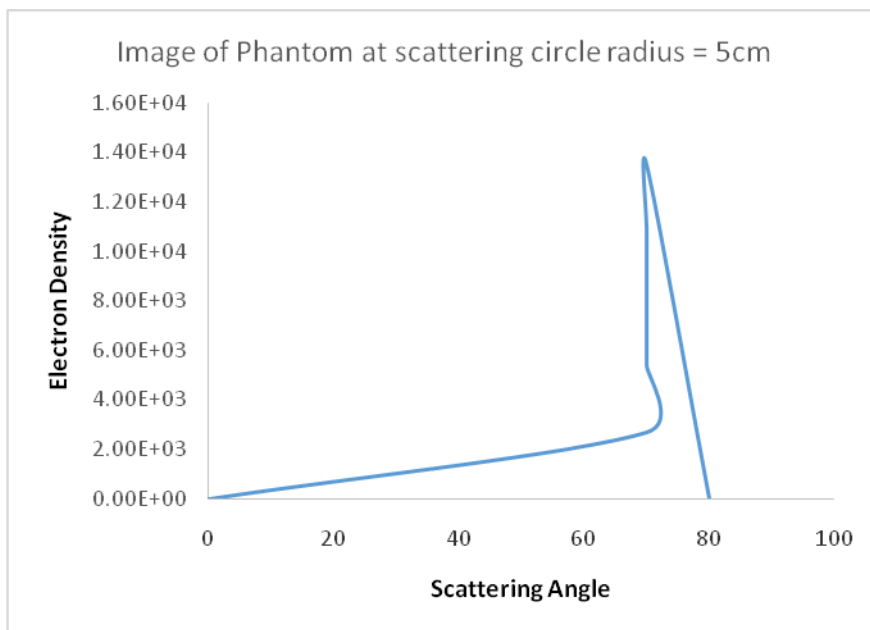


Fig. 1 Image of a Phantom at scattering circle radius, 5cm

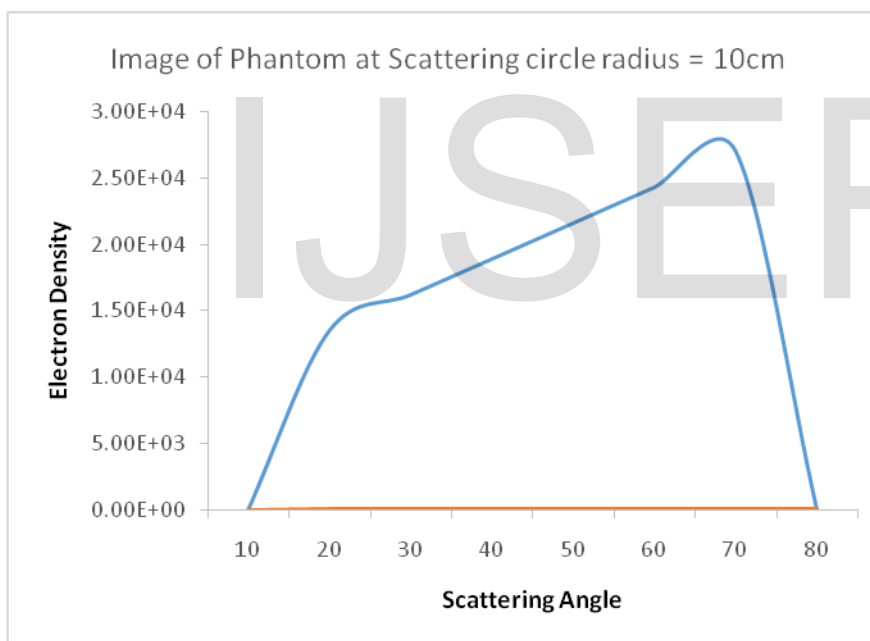


Fig. 2 Image of a Phantom at scattering circle radius, 10cm

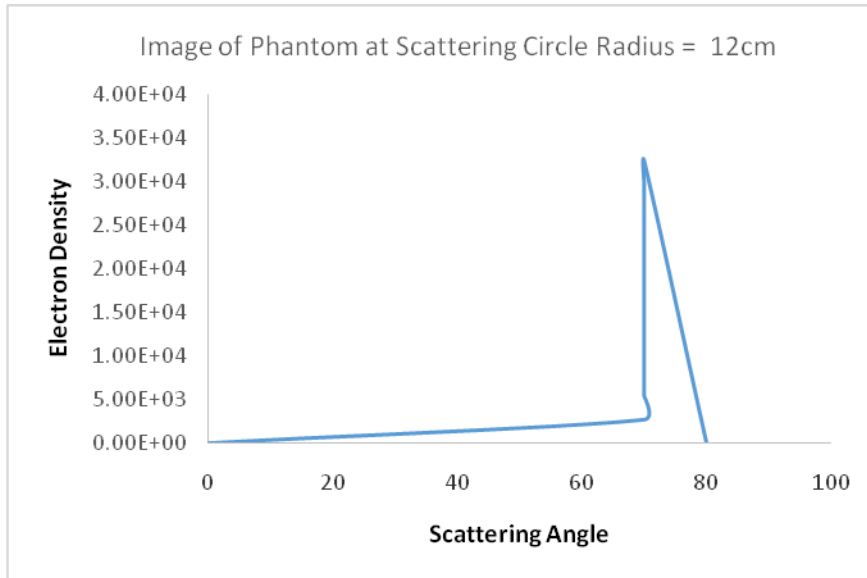


Fig. 3 Image of a Phantom at scattering circle radius, 12cm

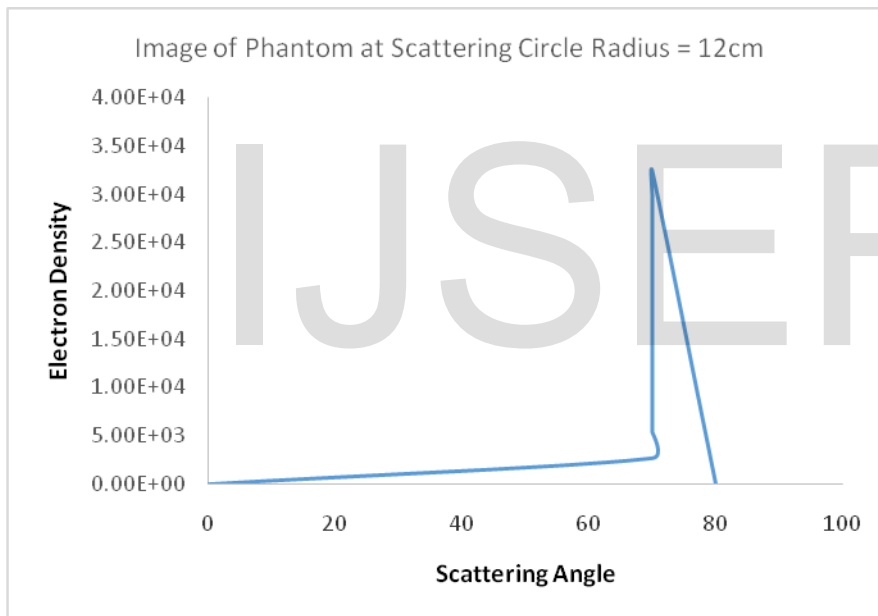


Fig. 4 Image of a Phantom at scattering circle radius, 13cm

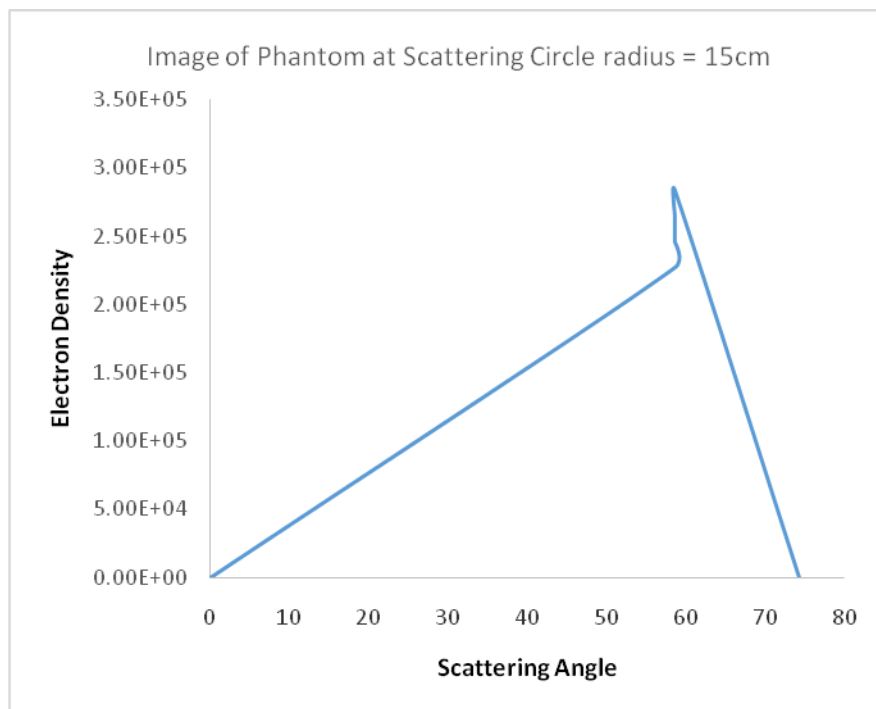


Fig. 5 Image of a Phantom at scattering circle radius 15cm

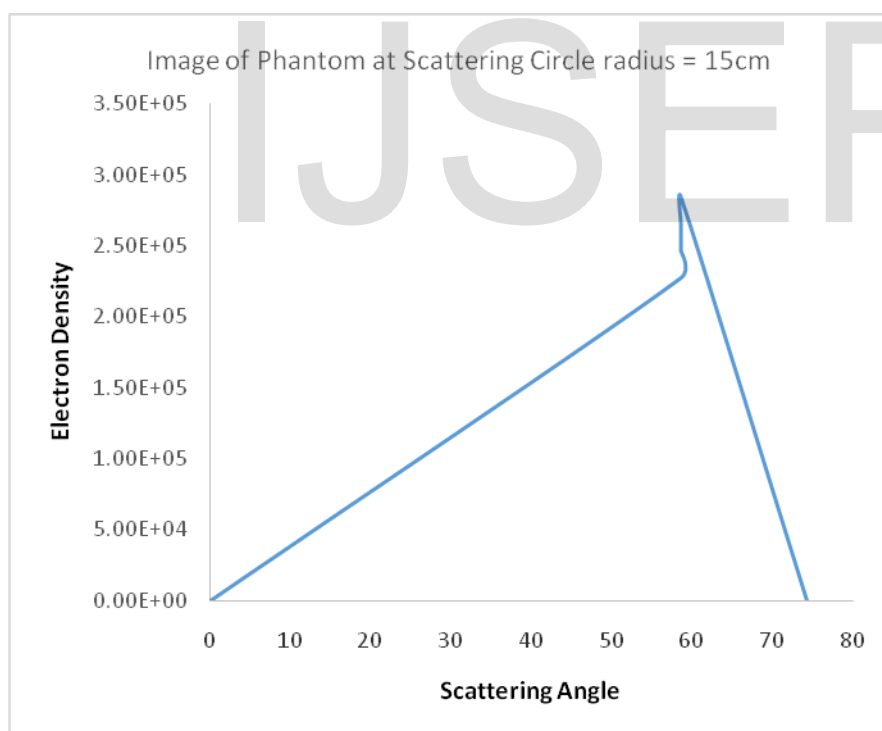


Fig. 6 Image of a Phantom at scattering circle radius 20cm

For real-time situations, the scattering circle radii may be varied by appropriately moving the radionuclide-detector frame to scan the object to be imaged. This can be achieved using a motion-controlled positioning system attached to the radionuclide-detector frame.

#### 4. Discussion

In Compton Scattering Tomography, the local Compton Scattering cross-section depends on the material's mass density and composition and is related to the local electron density of the material. In this work, images of a phantom were reconstructed by computing the electron density distribution data from a hypothetical object. In CST, the problem of attenuation is complicated and therefore, as a first approximation, uniform attenuation was assumed and the attenuation coefficient was assumed as not spatially dependent, but rather considered as dependent on energy in a known way (Hubbell et al., 1975). Norton, 1994 in his paper "Compton Scattering Tomography" considered a single scatterer before arriving at equation 2, and the approximate treatment of attenuation considered the case in which the weighting function was non-factorisable. A possible strategy for dealing with non-linear attenuation problem is to start with the assumption of a constant attenuation and then reconstruct the object function  $f_a(r, \theta_p)$  incorporating the weighting function,  $\omega$ . The resulting reconstruction of  $f_a(r, \theta_p)$  can then be substituted into the attenuation factor to give a new correction factor which can, in turn, be incorporated again into  $\omega$  and the process iterated until it "possibly" converges. This is a subject of future research on this topic.

By varying the scattering circle radii from the developed image reconstruction computer code, different versions of the image were obtained. A close examination of these varying versions reveals a somewhat good image (judging by the revelation of a greater image detail) at scattering circle radius of 10cm. Further investigation of this claim should be carried out practically when the real-life CST system is finally developed to authenticate the results obtained by this computer modeling. The practical implication of this should lead to the realization of optimal positioning of the source-detector frame for real-life object scans.

## References

- Adejumo, O.O., Balogun, F.A. and Egbedokun, G.G.O. (2011), "Developing a Compton Scattering Tomography System for Soil Studies: Theory", *Journal of Sustainable Development and Environmental Protection*, Vol. 1 No. 3, pp. 73-81.
- Arendtsz, N.V. and Hussein, E.M.A. (1995), "Energy Spectral Compton Scatter Imaging ---- Part I: Theory and Mathematics", *IEEE Transactions on Nuclear Science*, Vol. 42 No. 6, pp. 2155-2165.
- Cebeiro, J., Nguyen, M.K., Morvidone, M.A. and Noumowe, A. (2017), "New "improved" Compton Scatter Tomography Modality for Investigative Imaging of one-sided large objects", *Inverse Problems in Science and Engineering*, Taylor and Francis, Vol. 25 No. 11, pp. 1676-1696.
- Clarke, R.L., Milne, E.N.C. and Van Dyk, G. (1976), "The use of Compton Scattered Gamma Rays for Tomography", *Investigative Radiology*, Vol. 11, pp. 225-235.
- Farmer, F.T. and Collins, M.P. (1971), "A new approach to the Determination of anatomical cross-sections of the body by Compton Scattering of Gamma Rays", *Phys. Med. Bio.*, Vol. 16 No. 4, pp. 577-586.
- Hubbell, J.H., Veigele, W.J., Briggs, E.A., Brown, R.T., Cromer, D.T. and Howerton, R.J. (1975), "Atomic Form Factors, Incoherent Scattering Functions, and Photon Scattering Cross Section", *NIST Standard Reference Database Journal of Physical and Chemical Reference Data Reprints*, Vol. 4 No. 3, pp. 471-538.
- Kouris, K., Spyrou, N.M. and Jackson, D.F. (1982), *Imaging with Ionizing Radiations*, Progress in Medical and Environmental Physics, Vol. 1, Surrey University Press/Blackie, Glasgow and London.



- Lale, P.G (1959), “The Examination of Internal Tissues Using Gamma-Ray Scatter With a Possible Extension to Mega-Voltage Radiography”, *Phys. Med. Bio.*, Vol. 4, pp. 159-167.
- Norton, S.J (1994), “Compton Scattering Tomography”, *J. Appl. Phys.*, Vol. 76 No. 4, pp. 2007-2015.
- Wang, J., Chi, Z. and Wang, Y. (1999), “Analytic Reconstruction of Compton Scattering Tomography”, *J. Appl. Phys.*, Vol. 86 No. 4, pp. 1693-1698.

IJSER

## Appendix

### *Code for Compton Scattering Imaging Implementation*

```

#include <iostream>
#include <cmath>
using namespace std;
main()
{
double pi, phi[20], theta, R, r0[20], mu[20],
a[20], expa[20], Rexpa[20], h[20], d[20], b[20], f[20];
charcf, cphi;

inti, j, k, thetap, x, y;
pi = 1;

for (i=0; i<=180; i+=10)
//
{theta=(pi)*i;
phi[i] = (90) - theta;
}
// Define R (radius of scattering circle)
j=1;
for (y=1; y<=200; y++){
R=y/10;
r0[j]=2*R*cos(theta - phi[y]);
mu[j]=2/r0[j];
a[j]=(-mu[j]*r0[j]*(sin(80)-sin(10))/cos(80-phi[y]));
expa[j]=exp(a[j]);
Rexpa[j]=R*expa[j];
// Define h as a filter function
h[j]=exp(sin(12.5/r0[j])*12.5/r0[j]); }
for(k=2; k<=20; k++){
x=k-1;
for (thetap=0; thetap<=180; thetap+=10)
{d[x]=r0[1]*(cos(thetap-phi[x])/cos(80-phi[x]));}
//
b[x]=(r0[k] - d[x])*(1/pow(cos(10-phi[x]),2))*h[k];
}
for(R=1; R<=15; R+=1){
cout<< "f[j]" << "          "; cout<< "phi[j]" <<endl;
for(j=1; j<=20; j++){
f[j]=R*Rexpa[j]*b[j];
//
cout<< f[j] << "          " <<phi[j] <<endl; }
}
}
}
    
```